Supporting Information

Stimuli-Responsive Metal-Organic Supercontainers as Synthetic Proton Receptors

Cheng-Zhe Sun,[†,§,Ω] Li-Ji Cheng,[†,§,Ω] Yupu Qiao, [‡,Ω] Li-Yi Zhang,[†] Zhong-Ning Chen,[*,†] Feng-Rong Dai[*,†] Wei Lin, [*,‖] and Zhenqiang Wang[*,‡]

[Ω] These authors contributed equally to this work.

[†] State Key Laboratory of Structural Chemistry, Fujian Institute of Research on the Structure of Matter, Chinese Academy of Sciences, Fuzhou, Fujian 350002, China. E-mail: dfr@fjirsm.ac.cn; Fax: (+86) 591-63173171

[‡] Department of Chemistry & Center for Fluorinated Functional Materials, University of South Dakota, 414 East Clark Street, Churchill-Haines Laboratories, Room 115, Vermillion, SD 57069, United States. E-mail: Zhenqiang.Wang@usd.edu; Fax: (+1) 605-677-6397.

[‖]Department of Chemistry, Northwestern University, Evanston, IL, 60208, United States. Email: Wei.Lin@northwestern.edu.

[§] University of Chinese Academy of Sciences, Beijing 100049, China.

Table S1. Crystallographic Data for Compounds **1-Co** and **1-Zn**.

	1-Co	**1-Zn**
Empirical formula	$C_{360}H_{304}Co_{16}N_8O_{84}S_{16}$	$C_{360}H_{304}Zn_{16}N_8O_{84}S_{16}$
Formula weight	7541.93	7644.97
Temperature (K)	100(2)	100(2)
Wavelength	0.71073 Å	0.71073 Å
Crystal system	Triclinic	Triclinic
space group	*P*-1	*P*-1
a (Å)	20.249(19)	20.5268(13)
b (Å)	24.77(2)	25.0518(16)
c (Å)	26.23(2)	26.6569(17)
α (°)	111.143(12)	111.239(3)
β (°)	90.835(13)	90.990(3)
γ (°)	102.933(13)	102.756(3)
V (Å^3)	11894(19)	12389.9(14)
Z	1	1
D(calcd) (g cm^{-3})	1.052	1.025
μ (Mo K_α) (mm^{-1})	0.672	0.884
F(000)	3872	3928
θ range (°)	1.578 - 25.000	2.031 - 24.999
Limiting indices	-24<=h<=24,	-24<=h<=24
	29<=k<=29,	-29<=k<=29
	31<=l<=31	-31<=l<=31
Reflections	95530 / 39594	248803 / 43590
collected / unique	[R_{int} = 0.0754]	[R_{int} = 0.0384]
Data / restraints / parameters	39594 / 1020 / 2179	43590 / 612 / 2379
GOF	1.090	1.045
R_1 (I>2σ(I))	0.1155	0.0460
wR_2 (I>2σ(I))	0.3017	0.1295
R_1 (all data)	0.1613	0.0586
wR_2 (all data)	0.3441	0.1457
$\Delta\rho$ / e A$^{\circ -3}$	2.103, -0.982	1.075, -0.778

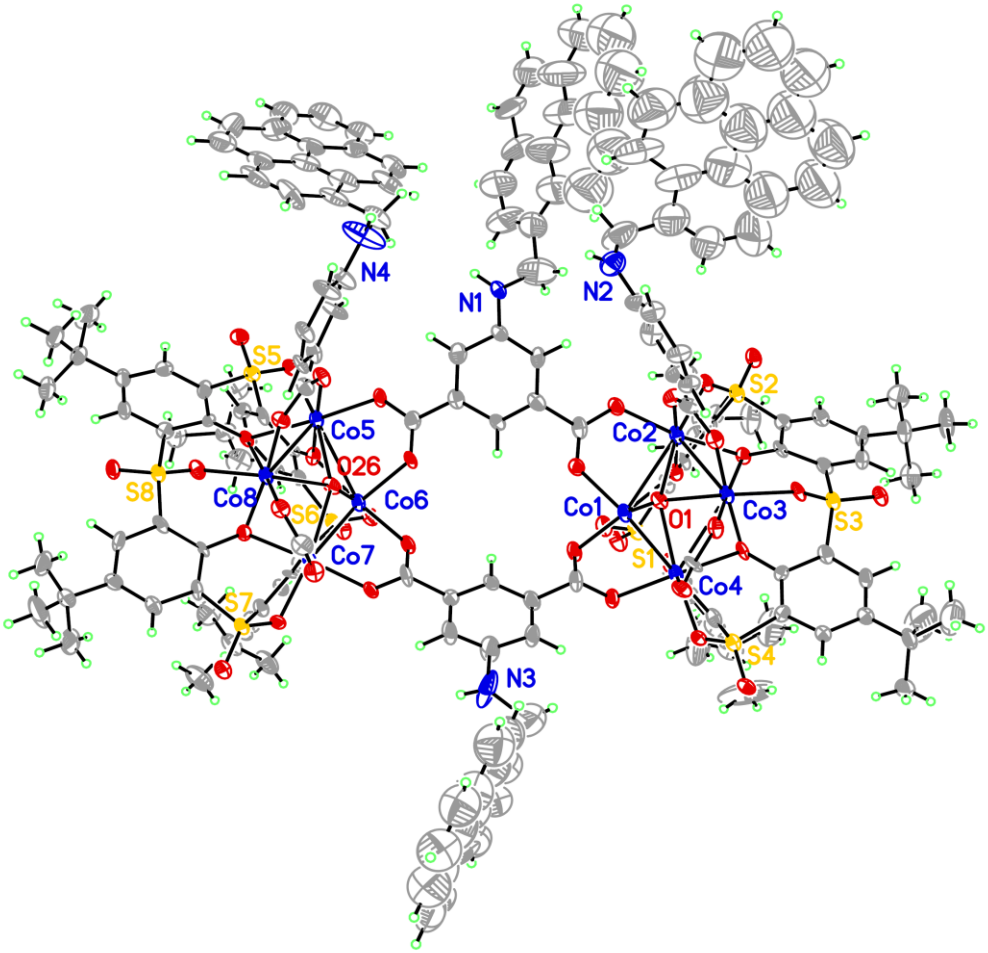

Figure S1. ORTEP drawing of the asymmetric unit of **1-Co** (thermal ellipsoids with 30% probability).

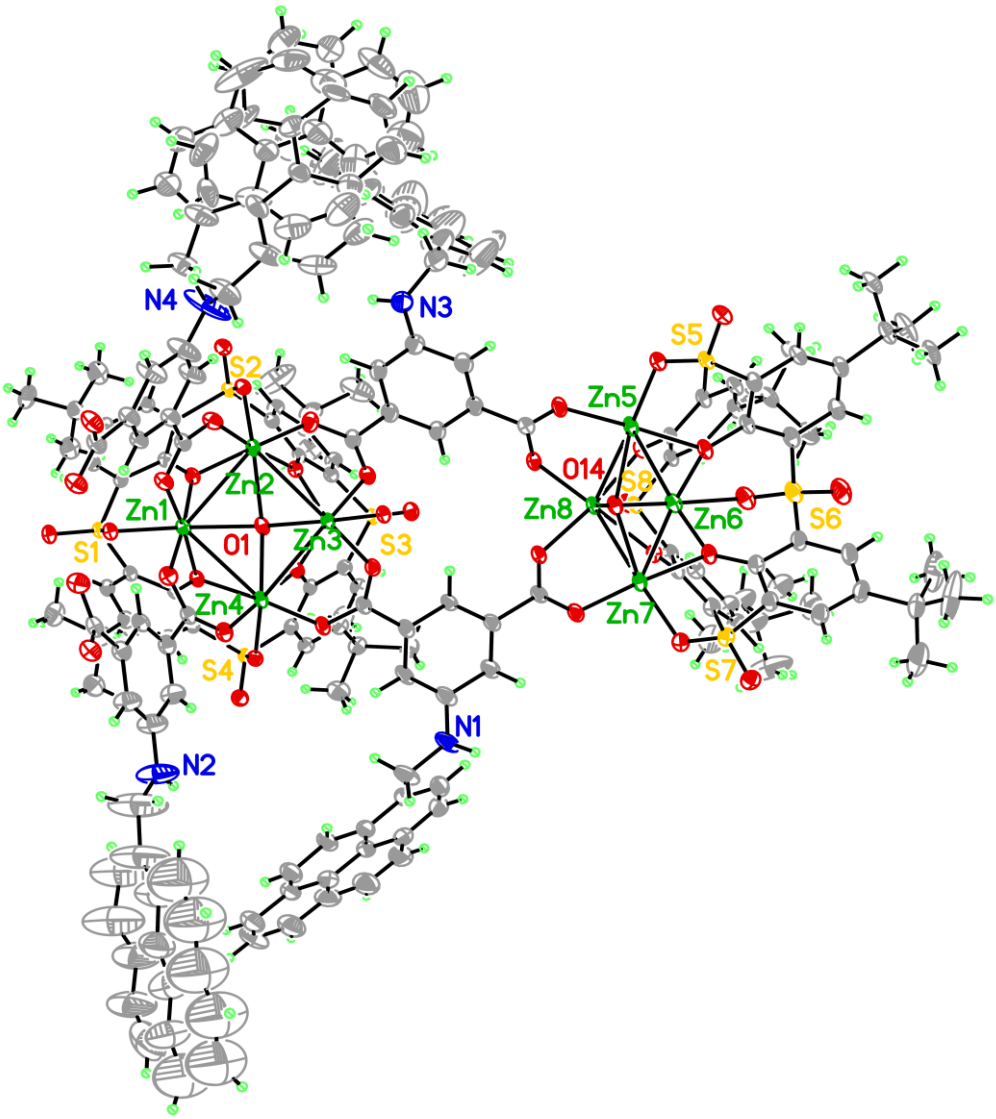

Figure S2. ORTEP drawing of the asymmetric unit of **1-Zn** (thermal ellipsoids with 30% probability).

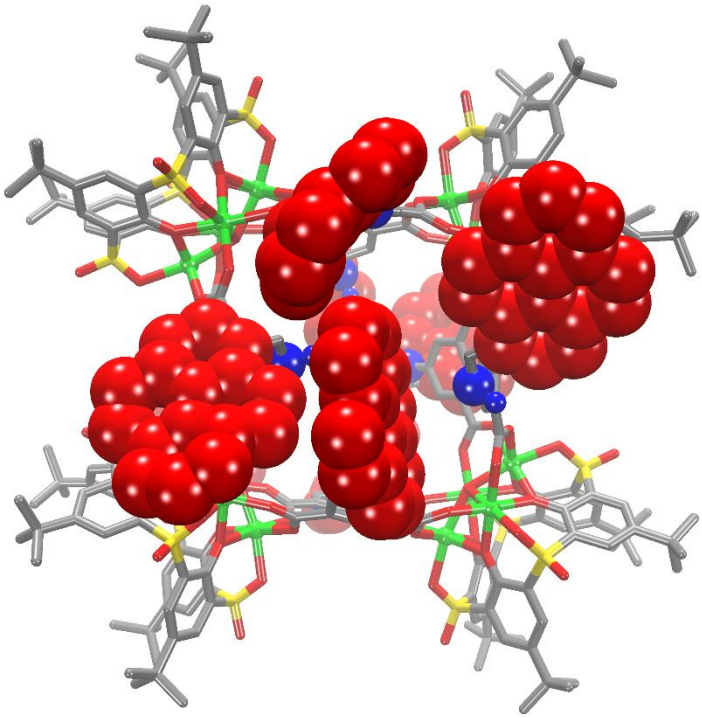

Figure S3. "*Edge-to-face*" *π-π* interactions between adjacent pyrenyl groups in **1-Co** and **1-Zn**.

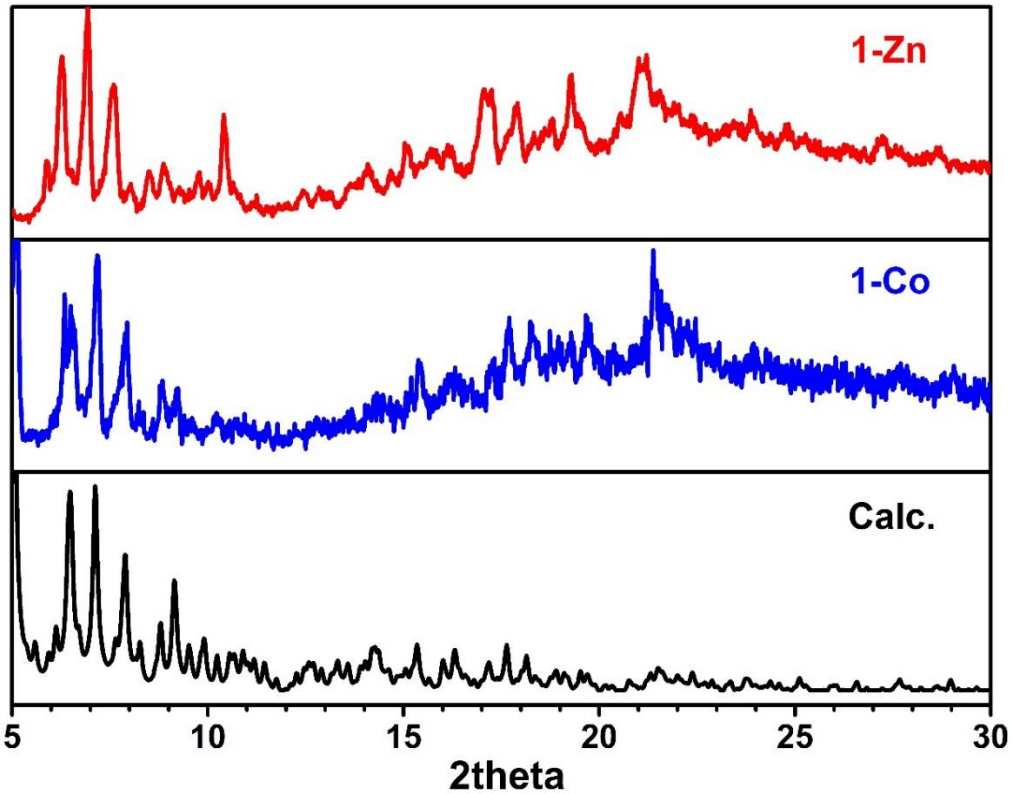

Figure S4. Experimental PXRD patterns of **1-Zn** (top) and **1-Co** (middle), in comparison with simulated pattern (bottom) calculated from single-crystal structures.

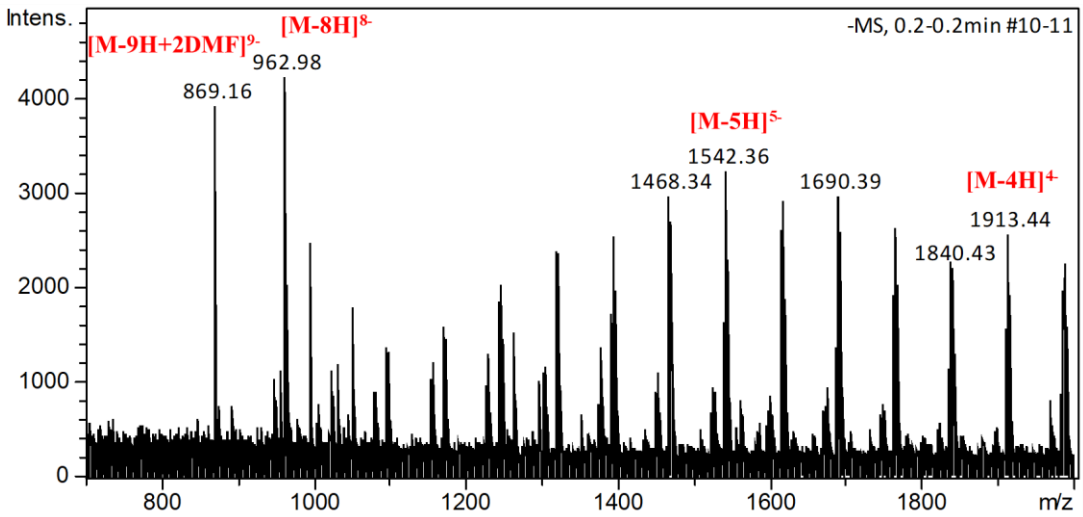

Figure S5. ESI-MS spectrum of **1-Zn** indicating the structural integrity in solution.

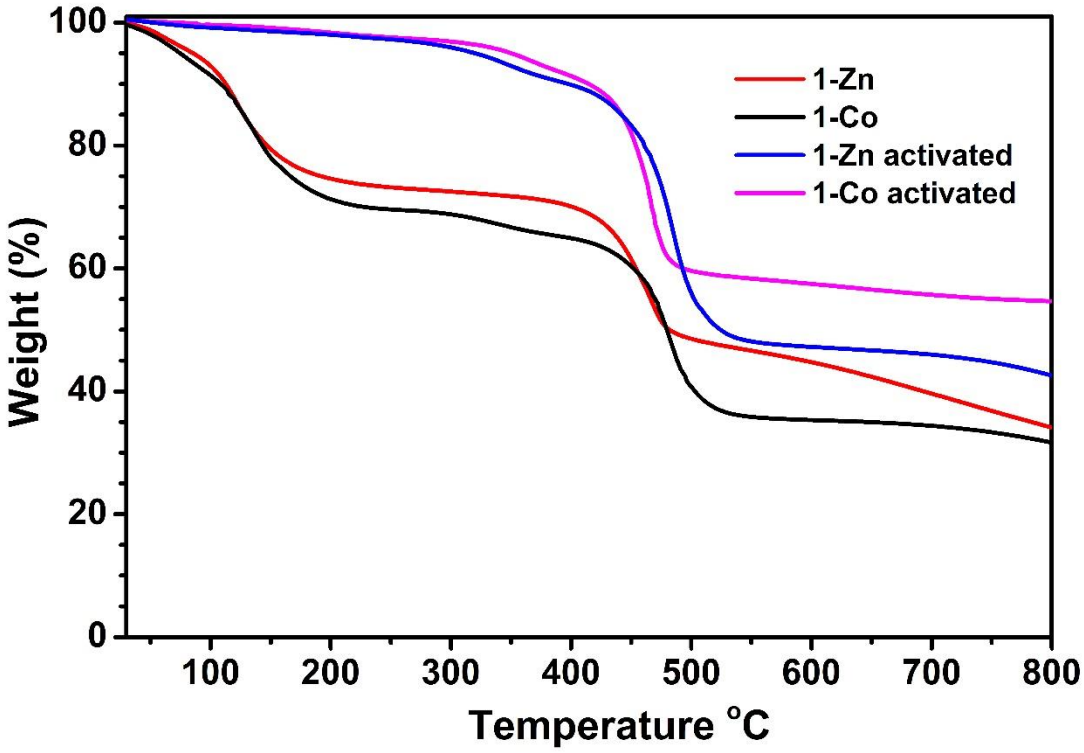

Figure S6. TGA of as-synthesized and activated samples of **1-Co** and **1-Zn**.

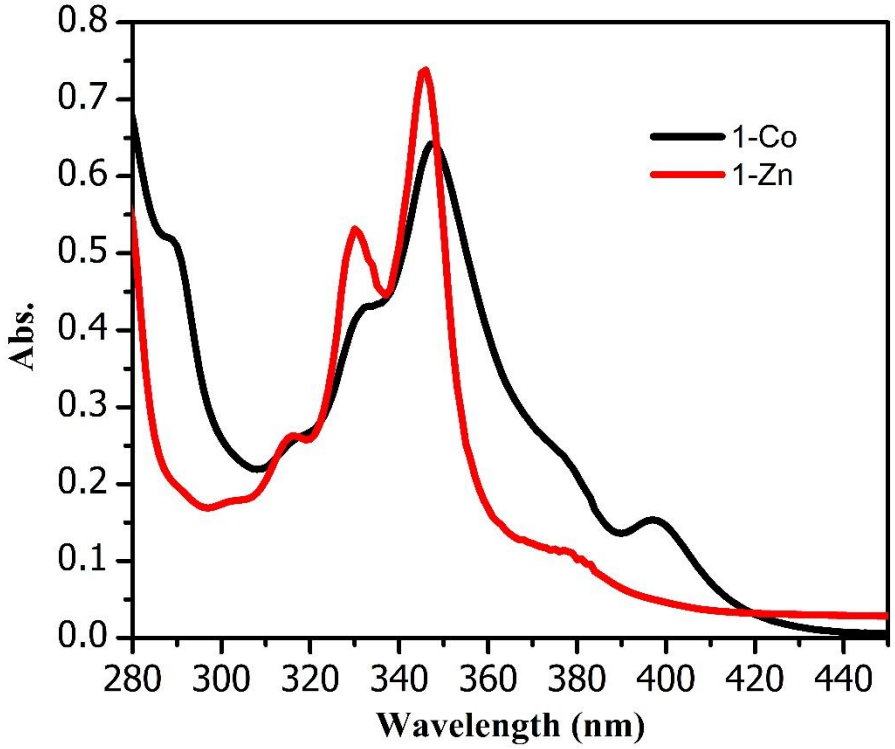

Figure S7. UV-vis absorption spectra of **1-Co** and **1-Zn** in $CHCl_3$ solution.

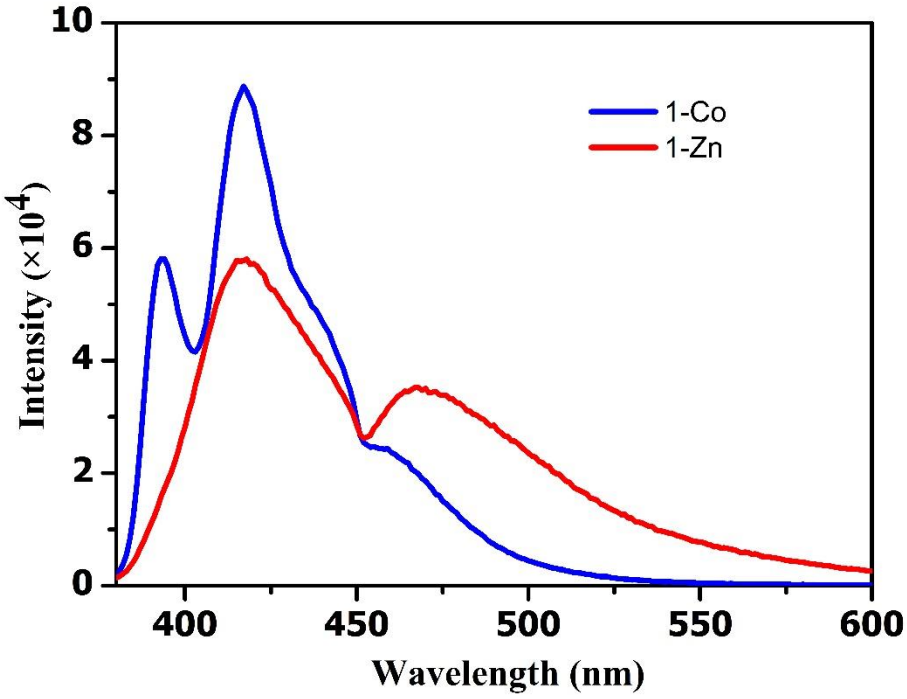

Figure S8. Emission spectra of **1-Zn** (red) and **1-Co** (blue) in $CHCl_3$.

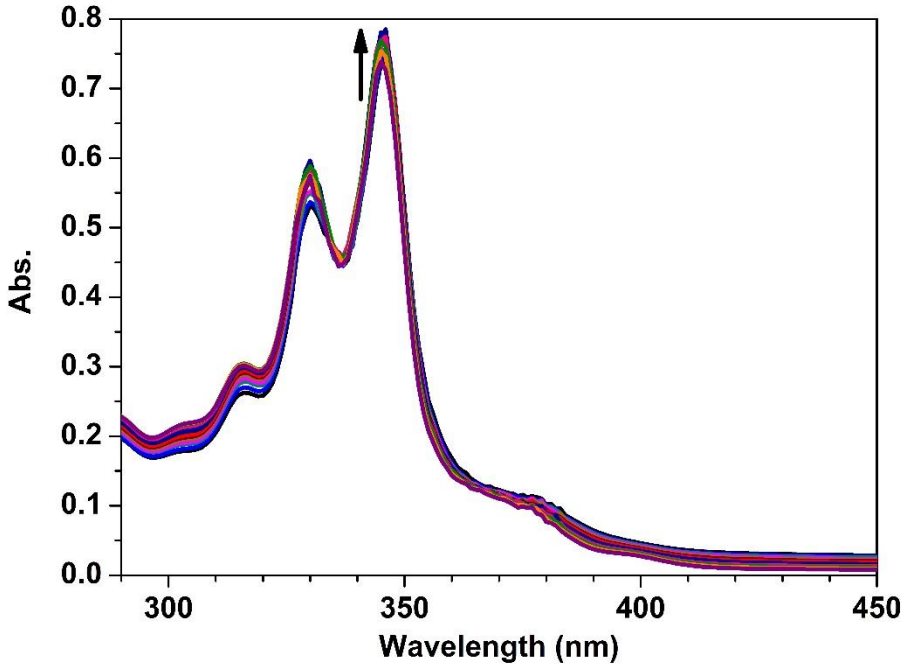

Figure S9. UV-Vis absorption spectra of **1-Zn** titrated with CF_3COOH. The arrow indicates a gradual increase of CF_3COOH equivalents.

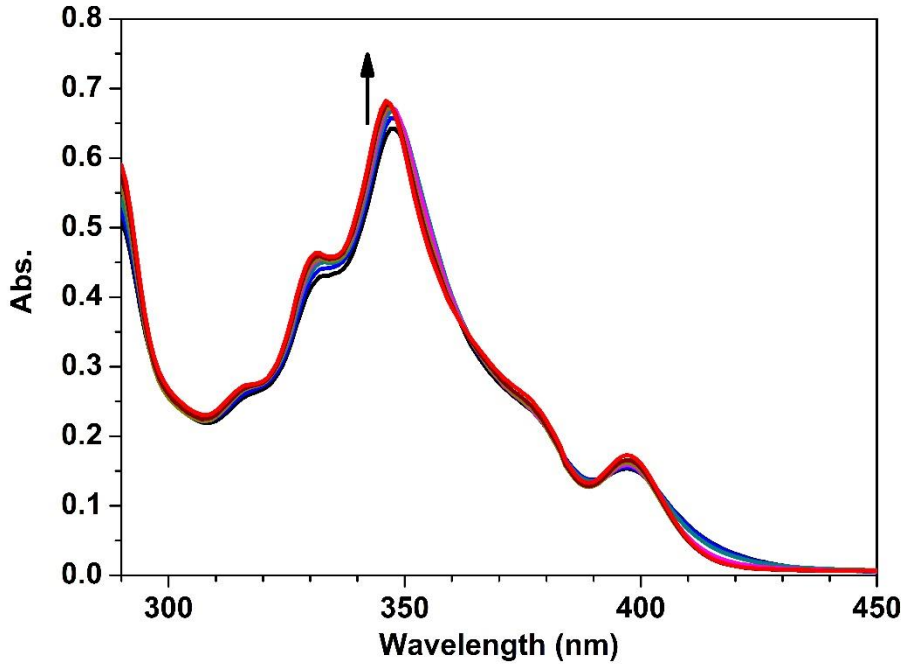

Figure S10. UV-Vis absorption spectra of **1-Co** titrated with CF_3COOH. The arrow indicates a gradual increase of CF_3COOH equivalents.

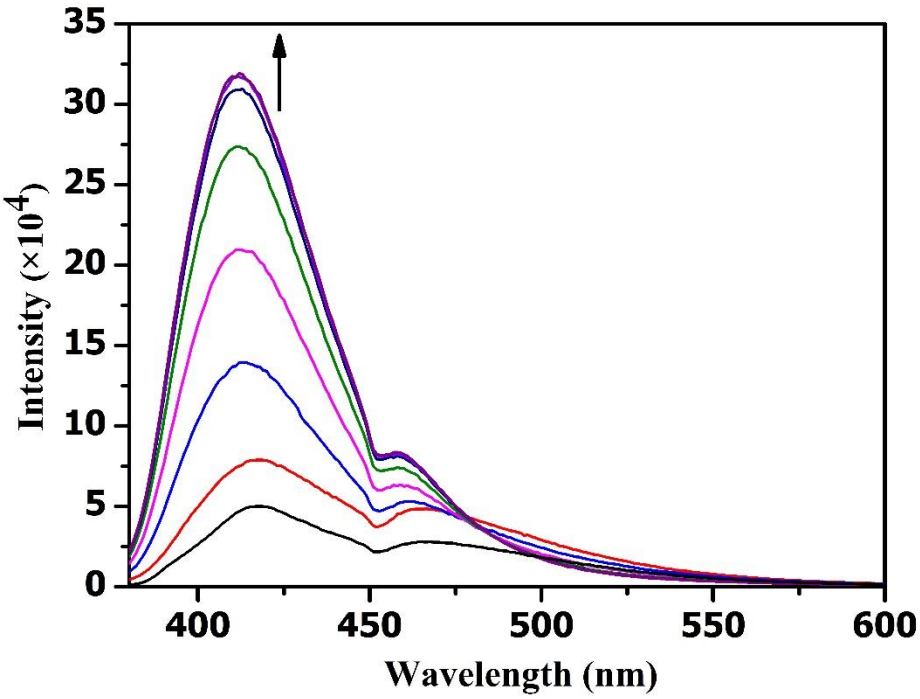

Figure S11. Emission spectra of **1-Zn** titrated with CF_3COOH. The arrow indicates a gradual increase of CF_3COOH equivalents.

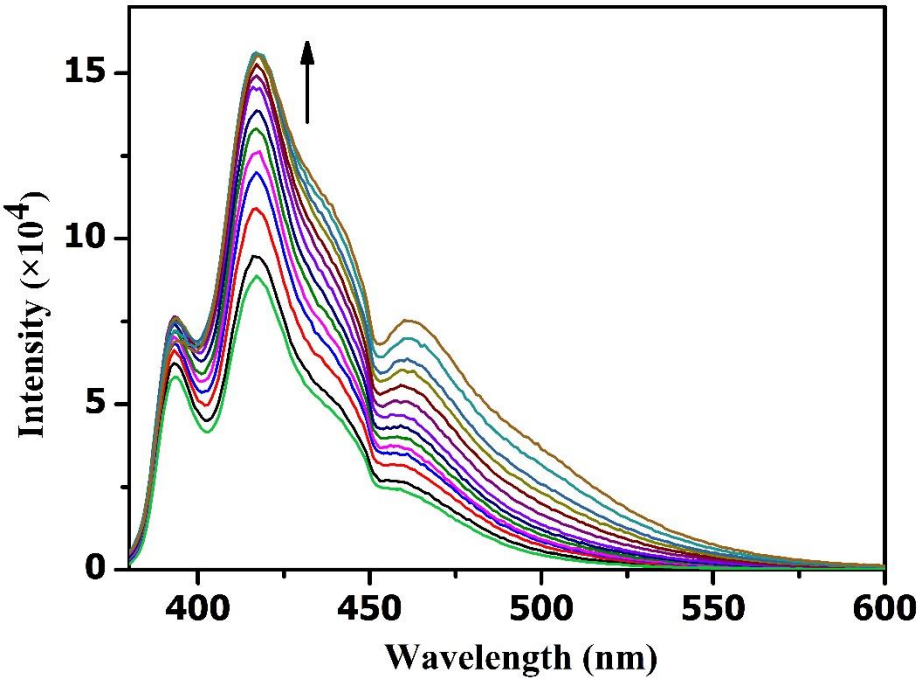

Figure S12. Emission spectra of **1-Co** titrated with CF_3COOH. The arrow indicates a gradual increase of CF_3COOH equivalents.

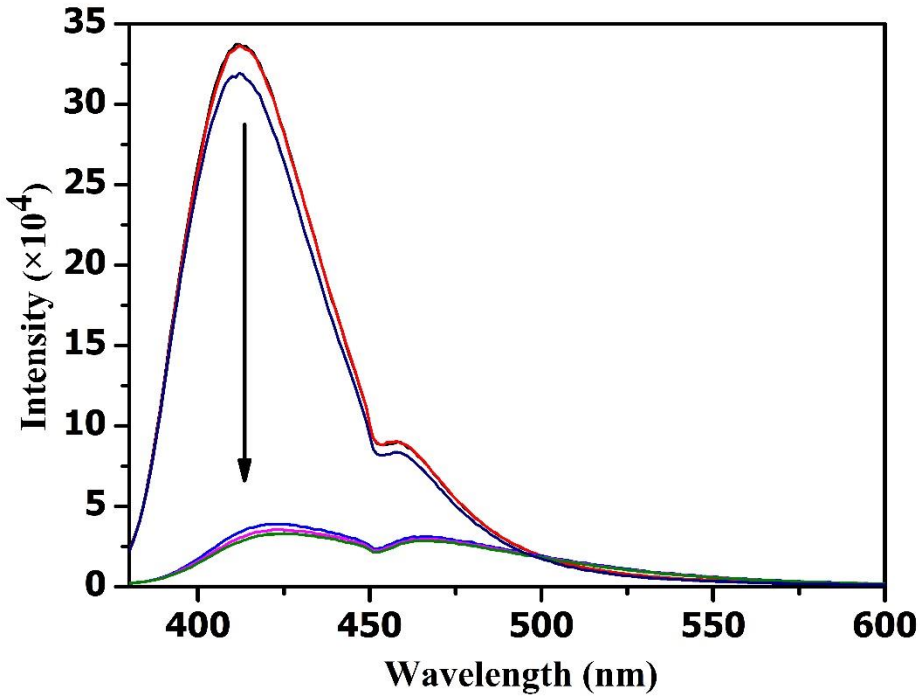

Figure S13. Emission spectra of a mixture of **1-Zn** and excess CF_3COOH titrated with Et_3N. The arrow indicates a gradual increase of Et_3N equivalents.

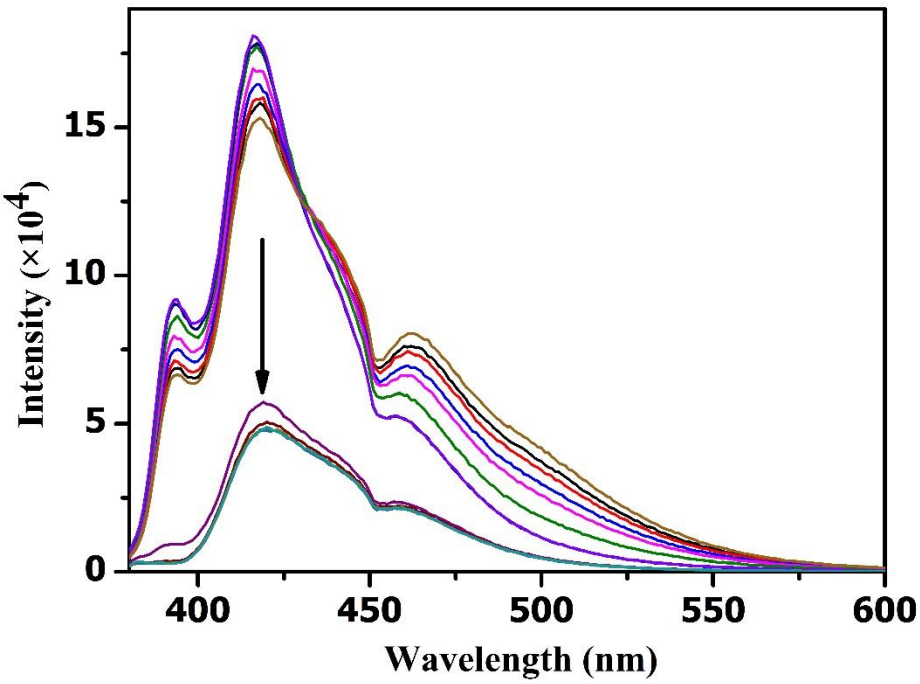

Figure S14. Emission spectra of a mixture of **1-Co** and excess CF_3COOH titrated with Et_3N. The arrow indicates a gradual increase of Et_3N equivalents.

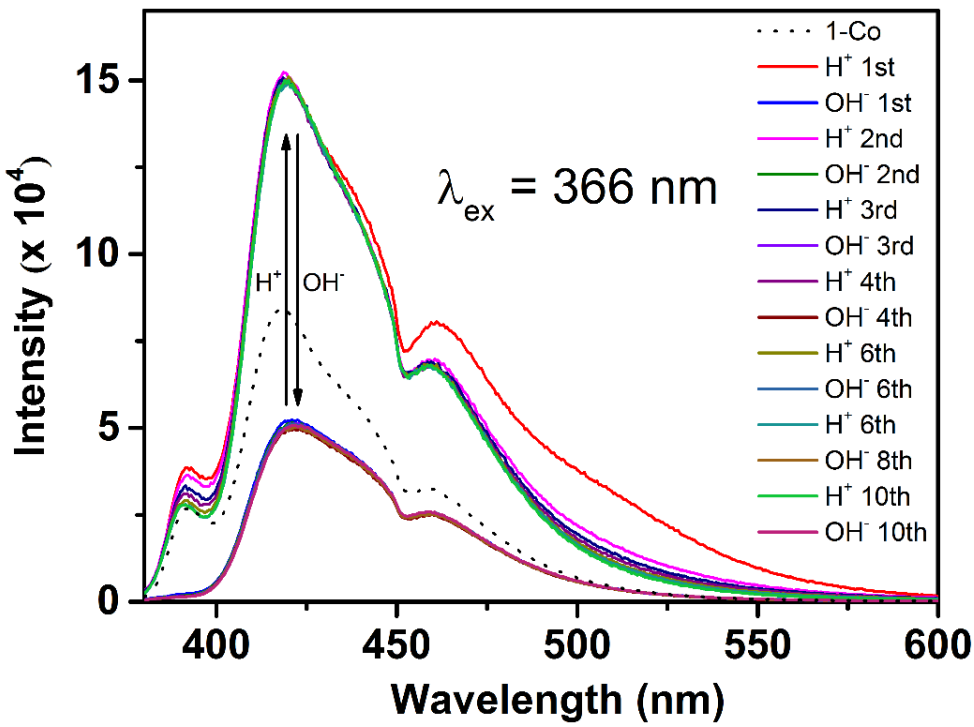

Figure S15. Switching "on" and "off" of **1-Co** with CF_3COOH/Et_3N can be repeated multiple cycles.

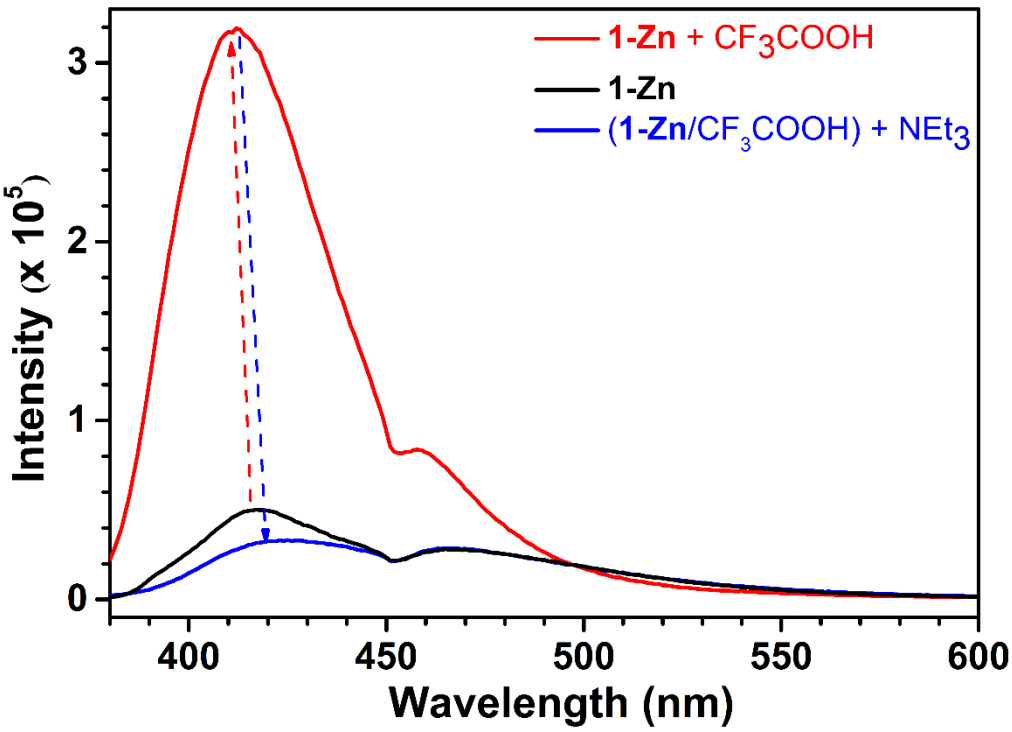

Figure S16. Fluorescence emission spectra of **1-Zn** (black), **1-Zn** added with excess CF_3COOH (red), and **1-Zn**/CF_3COOH treated with excess Et_3N (blue).

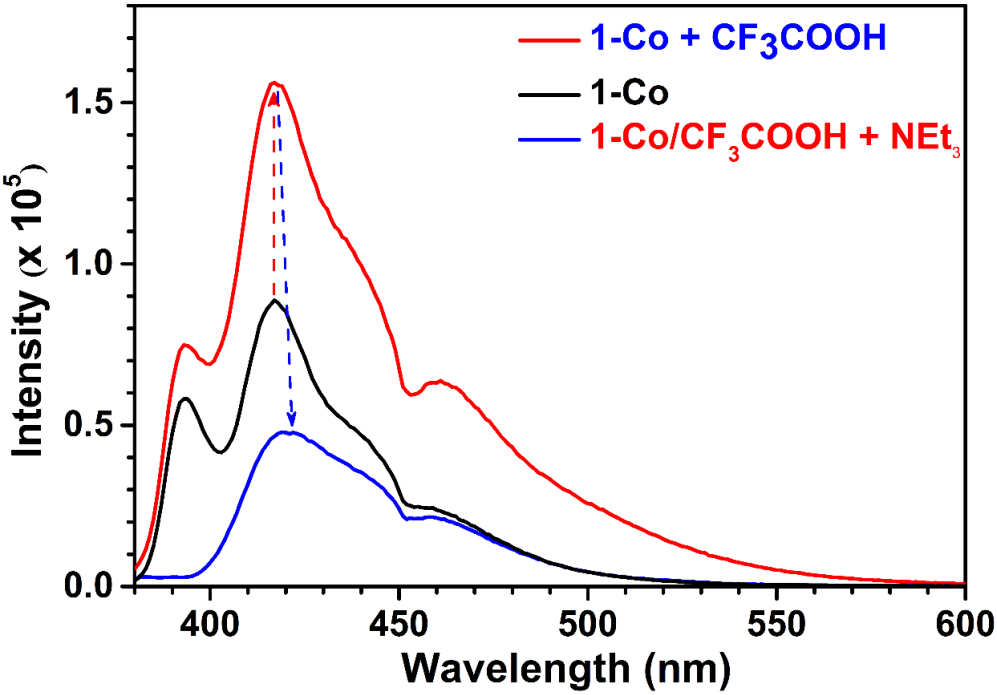

Figure S17. Fluorescence emission spectra of **1-Co** (black), **1-Co** added with excess CF_3COOH (red), and **1-Co**/CF_3COOH treated with excess Et_3N (blue).

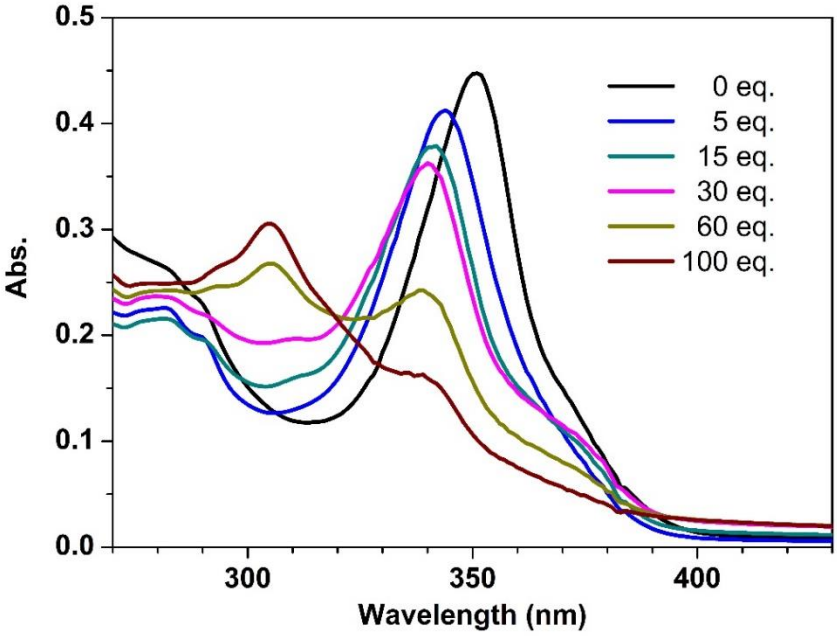

Figure S18. UV-Vis absorption spectra of a parent type-III MOSC ("MOSC-III-Co") titrated with CF_3COOH, indicating decomposition of the MOSC upon addition of a few CF_3COOH equivalents.

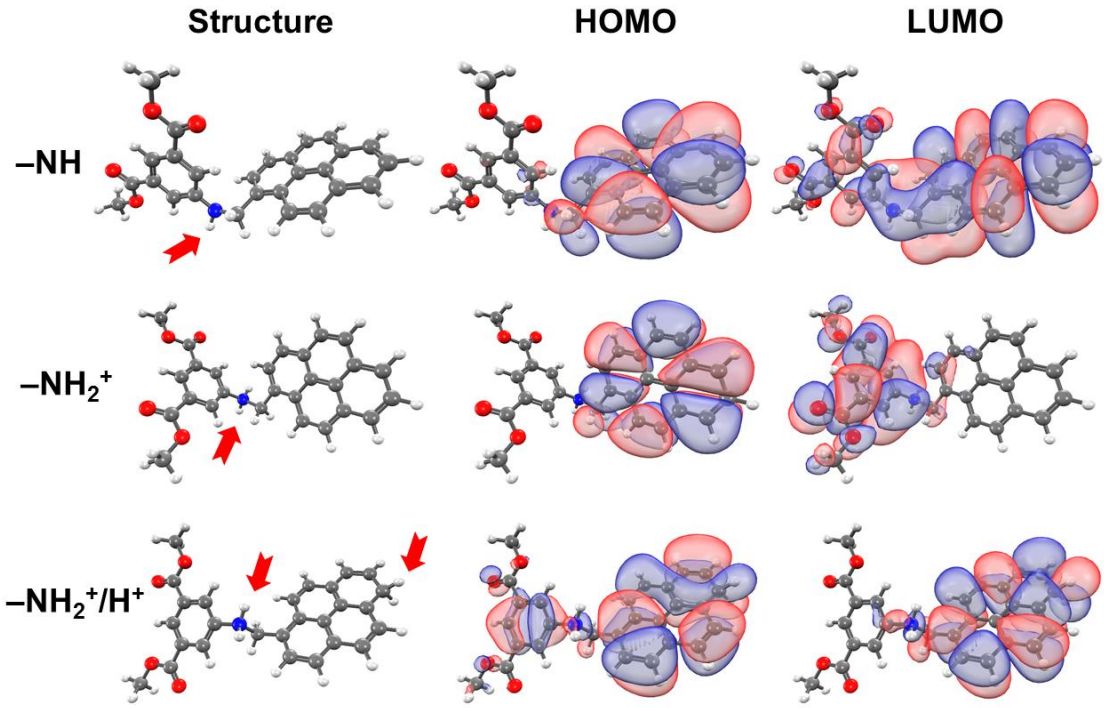

Figure S19. Density functional theory (DFT) calculation results obtained at the M06-L/aug-cc-pVTZ level, showing the highest-occupied molecular orbital (HOMO) and lowest-unoccupied molecular orbital (LUMO) of model compound Me_2-**L1** before (top) and after (middle) protonation at the –NH group, and additional protonation of the pyrenyl unit (bottom).

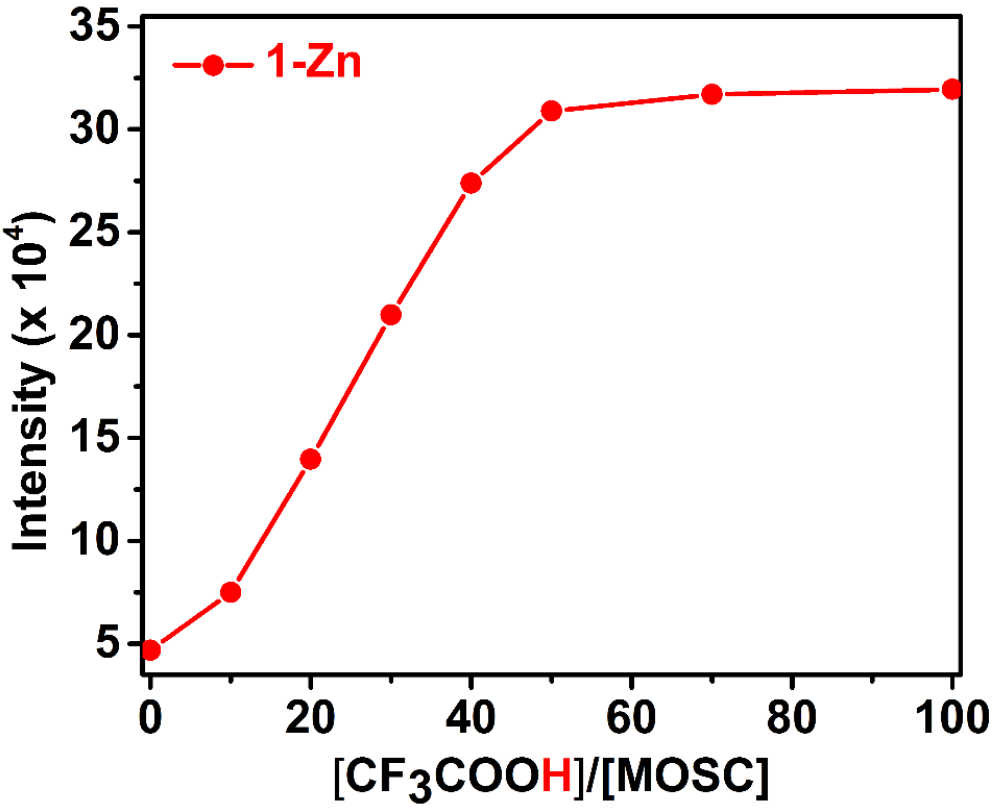

Figure S20. Plot of fluorescent intensity vs. CF_3COOH equivalents for the titration of **1-Zn** with CF_3COOH.

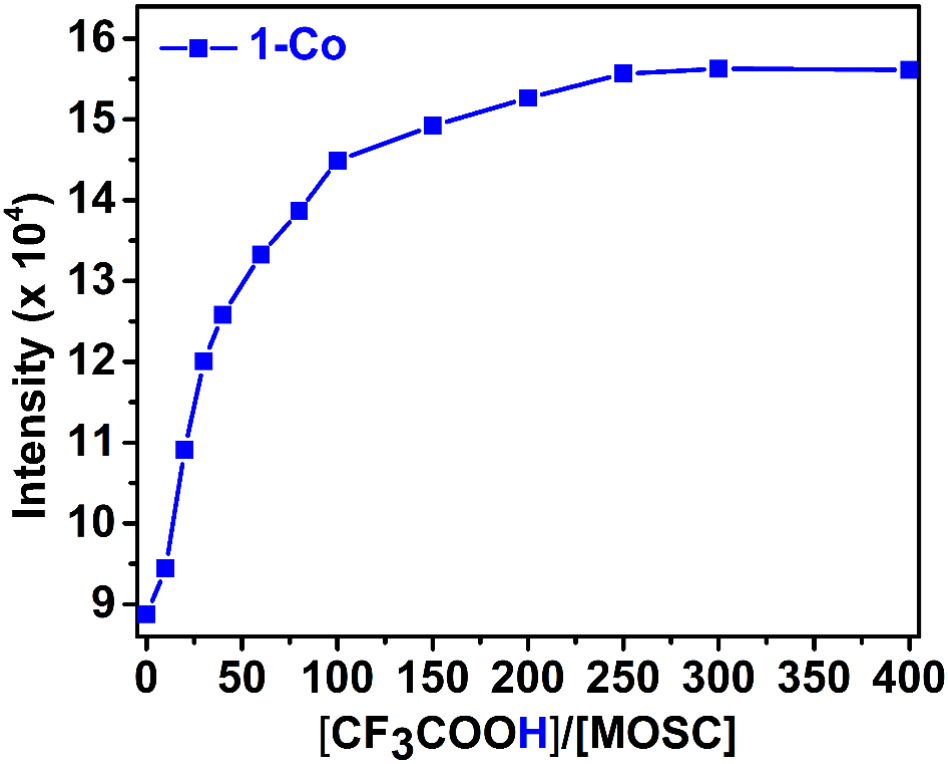

Figure S21. Plot of fluorescent intensity vs. CF_3COOH equivalents for the titration of **1-Co** with CF_3COOH.

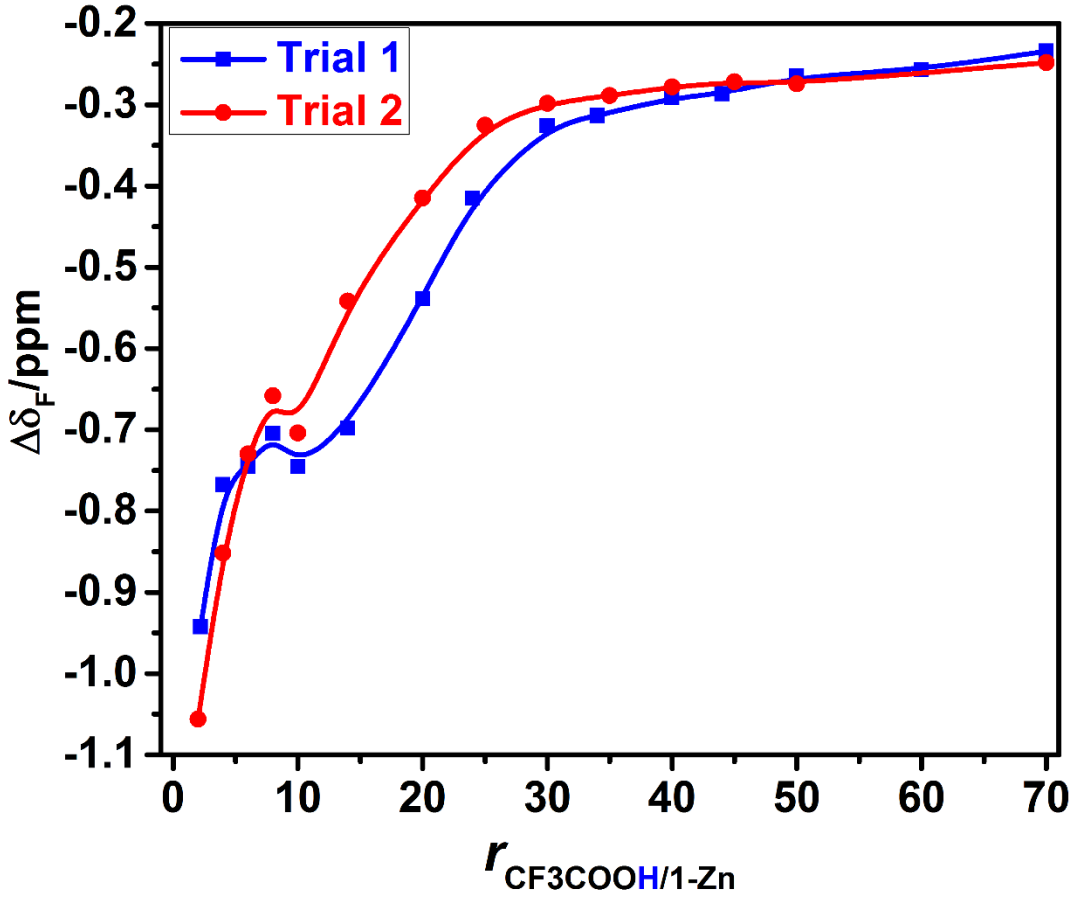

Figure S22. Two parallel ^{19}F NMR titration results, showing the correlation of up-field shifts of C**F**$_3$COO$^-$ ($\Delta\delta_F$/ppm) as a function of a gradual increase of C**F**$_3$COOH/**1-Zn** molar ratios.

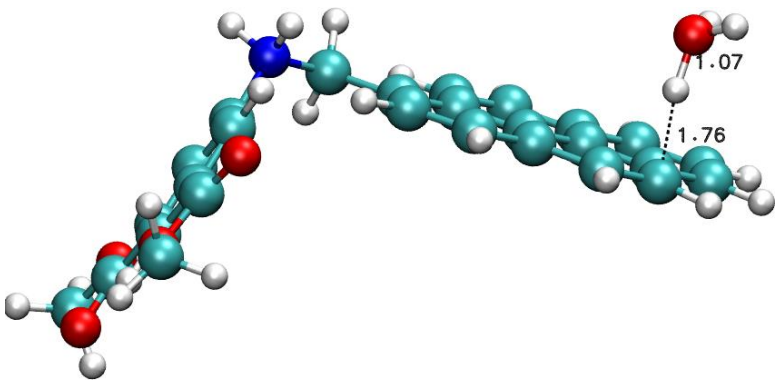

Figure S23. Hydrogen bonding between H_3O^+ ion and a peripheral carbon atom of the pyrenyl unit in *N-protonated* Me_2-**L1**.

***a*) -NH_2^+/2H_3O^+ (TYPE I)**

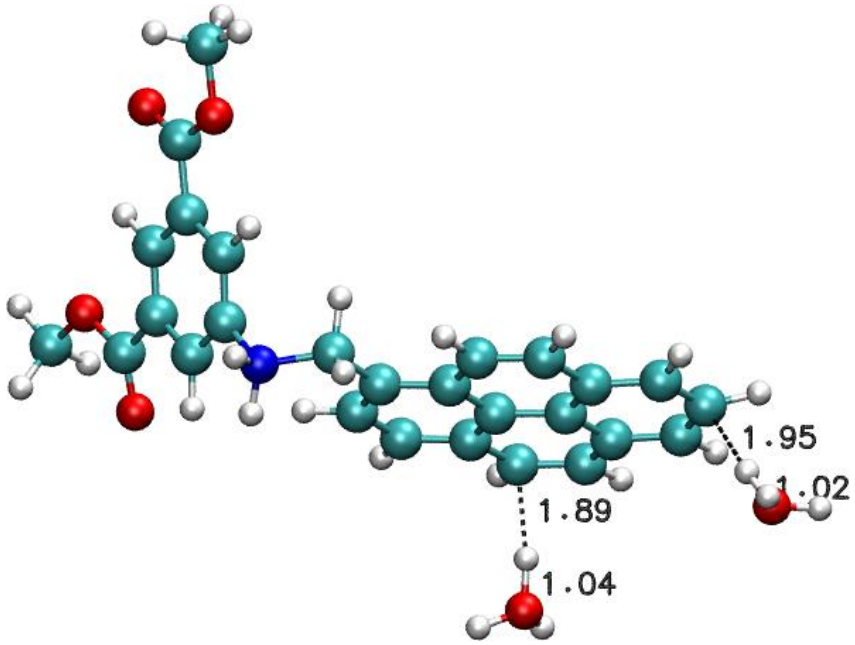

***b*) -NH_2^+/2H_3O^+ (TYPE II)**

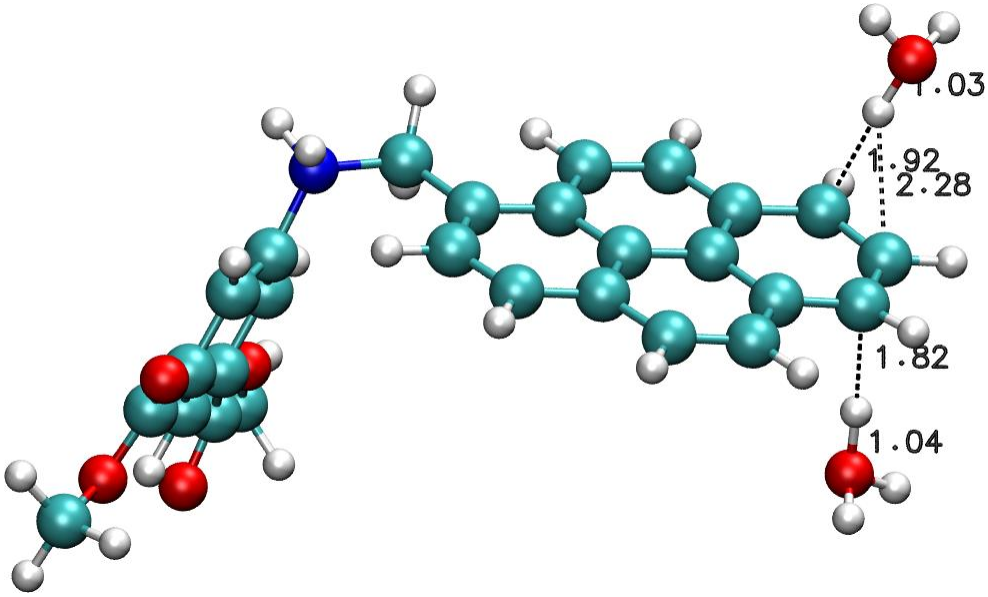

Figure S24. Two representative types of hydrogen bonding motifs between two H_3O^+ ions and peripheral carbon atoms of the pyrenyl unit in *N-protonated* Me_2-**L1** (–NH_2^+).

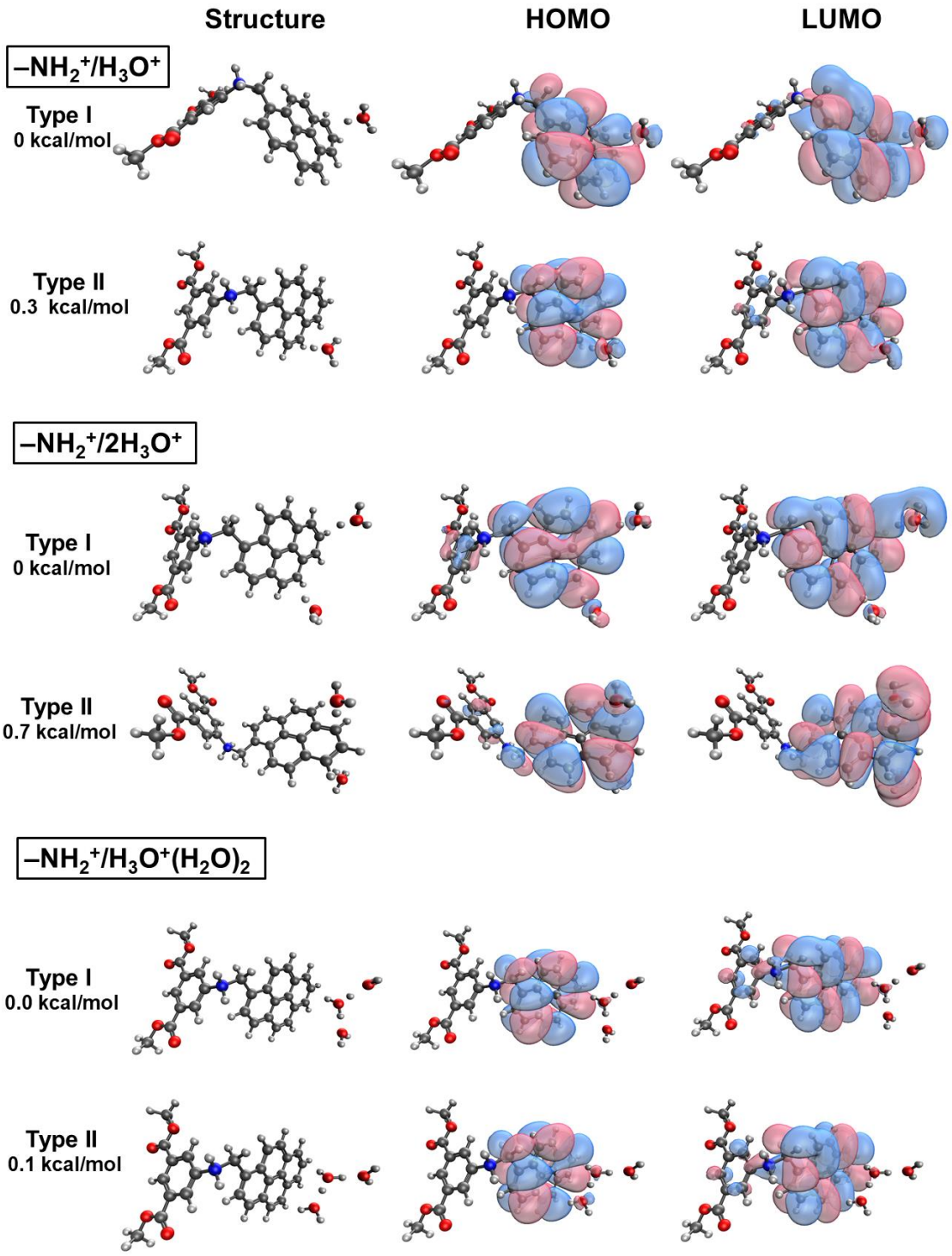

Figure S25. DFT calculation results obtained at the M06-L/aug-cc-pVTZ level, showing relative energies, structures, HOMO, and LUMO of the *N*-protonated model compound Me_2-**L1**($–NH_2^+$) binding with one H_3O^+ species, two H_3O^+ species, and one $H_3O^+(H_2O)_2$ species. The energies are relative to the lowest-energy states, which are arbitrarily set to be 0.0 kcal/mol.

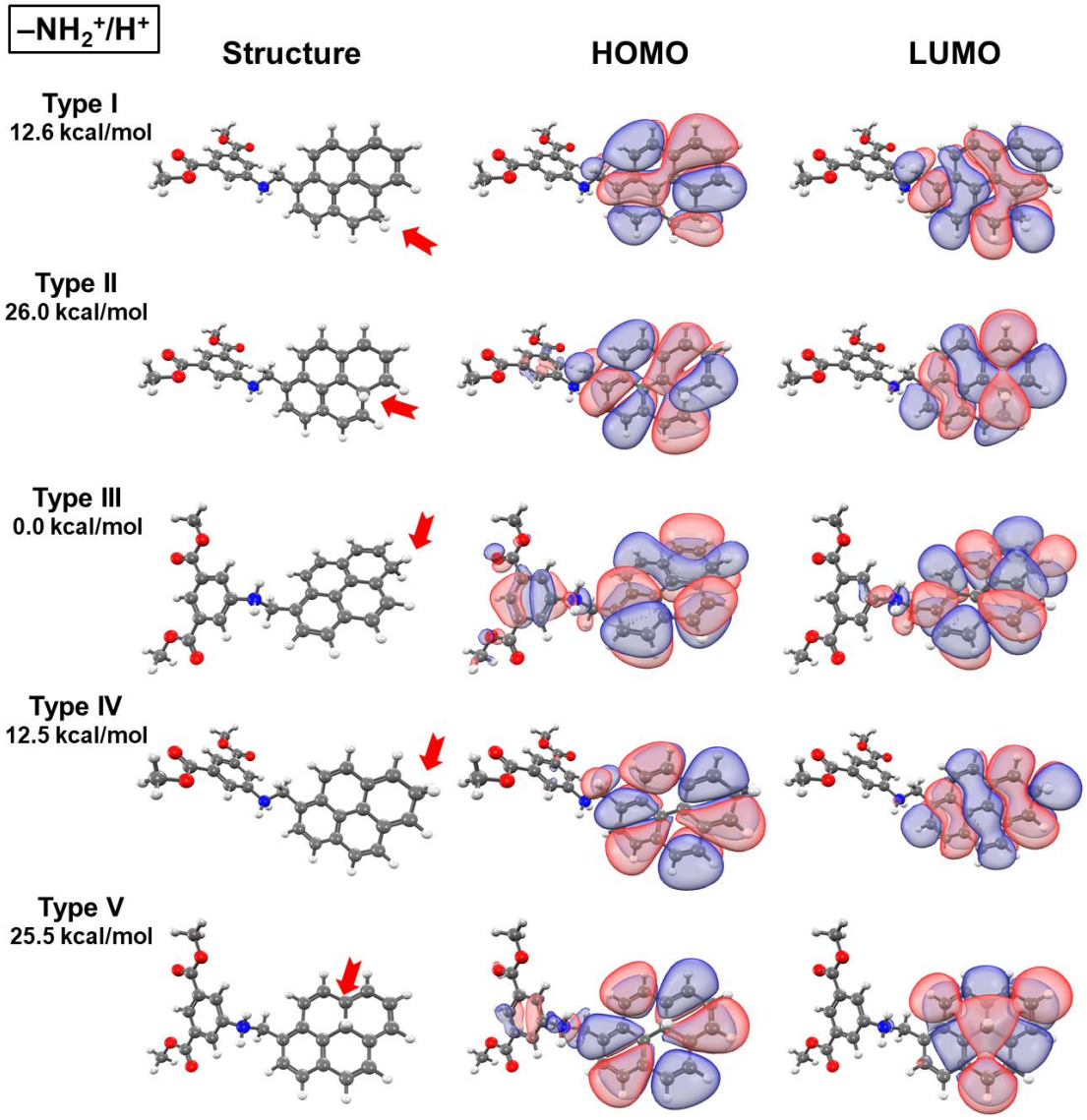

Figure S26. DFT calculation results obtained at the M06-L/aug-cc-pVTZ level, showing relative binding energies, HOMOs, and LUMOs of five possible H^+ binding sites, all of which form a *covalent* C-H bond at the pyrenyl units of the *N*-protonated model compound Me_2-**L1**($–NH_2^+$). The energies are relative to the lowest-energy state, i.e., binding site III, which is arbitrarily set to be 0.0 kcal/mol. The relative trend of these binding energies is consistent with recently reported results obtained at the RI-MP2/def2-TZVPP level.

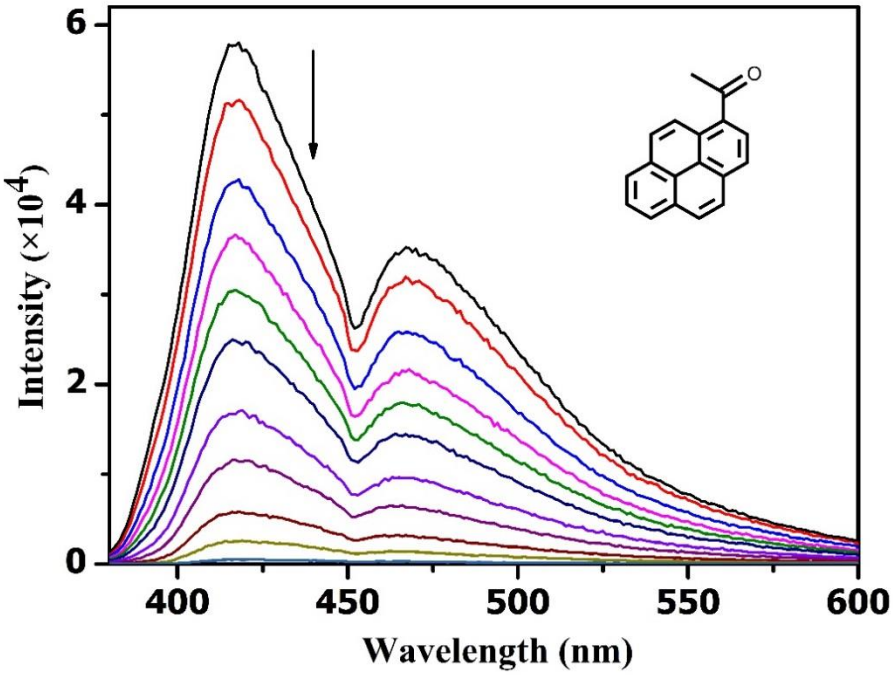

Figure S27. Emission spectra of **1-Zn** titrated with 1-acetylpyrene. The arrow indicates a gradual increase of 1-acetylpyrene equivalent.

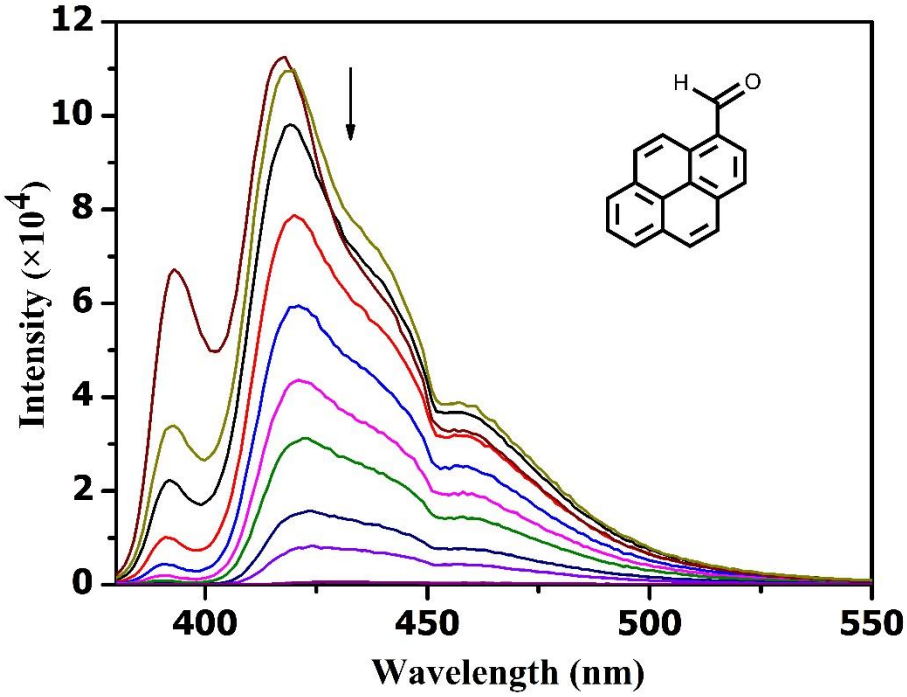

Figure S28. Emission spectra of **1-Co** titrated with 1-pyrenealdehyde. The arrow indicates a gradual increase of 1-pyrenealdehyde equivalent.

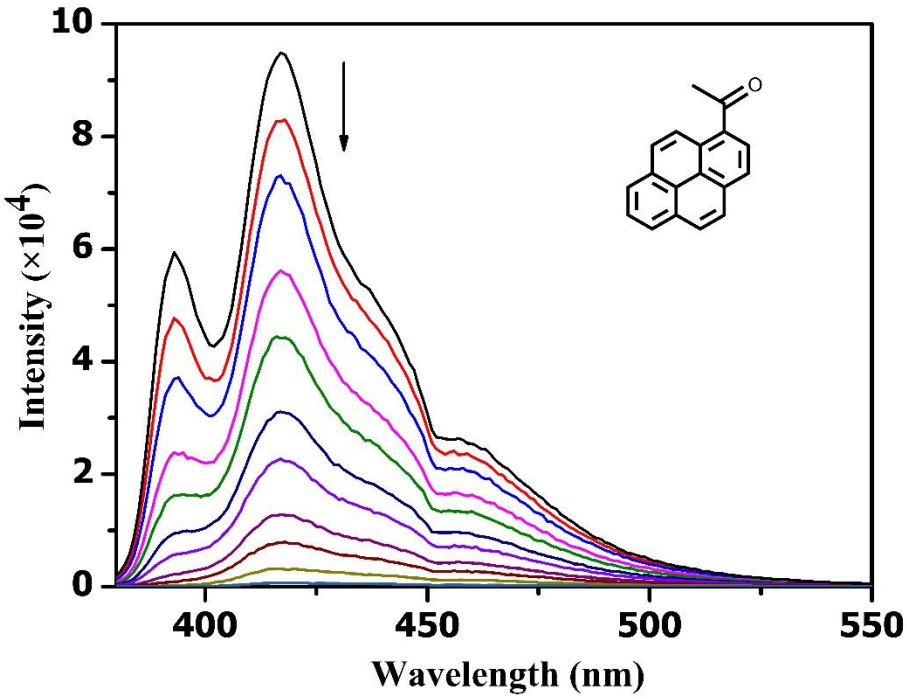

Figure S29. Emission spectra of **1-Co** titrated with 1-acetylpyrene. The arrow indicates a gradual increase of 1-acetylpyrene equivalent.

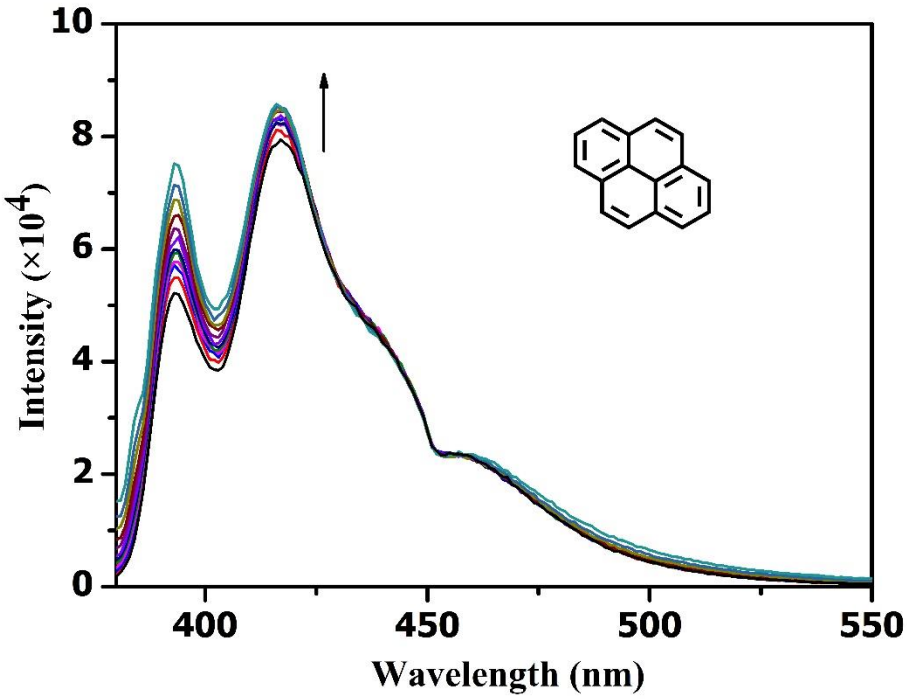

Figure S30. Emission spectra of **1-Co** titrated with pyrene. The arrow indicates a gradual increase of pyrene equivalent.

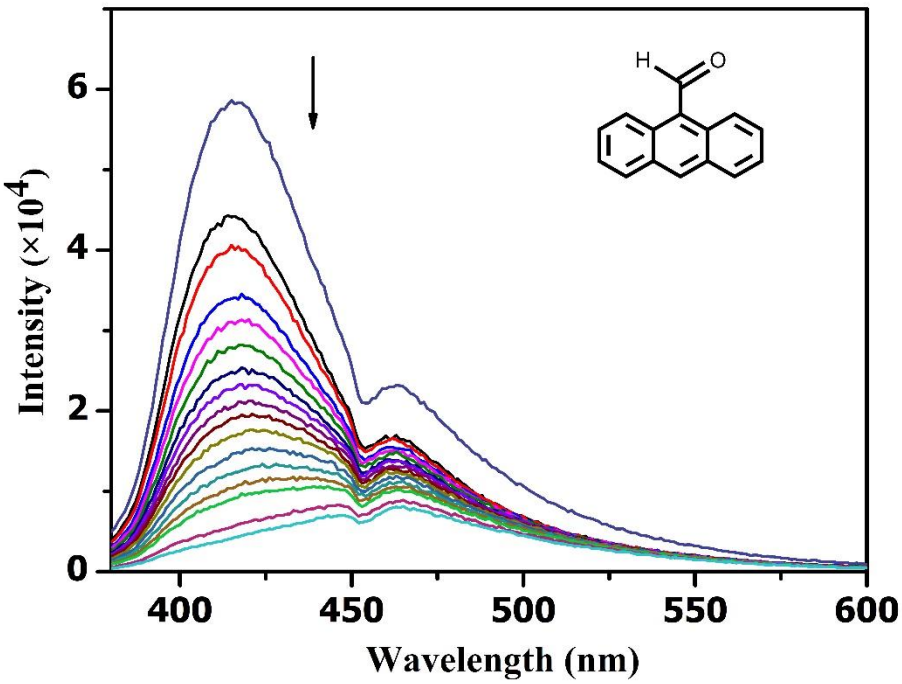

Figure S31. Emission spectra of **1-Zn** titrated with 9-anthraldehyde. The arrow indicates a gradual increase of 9-anthraldehyde equivalent.

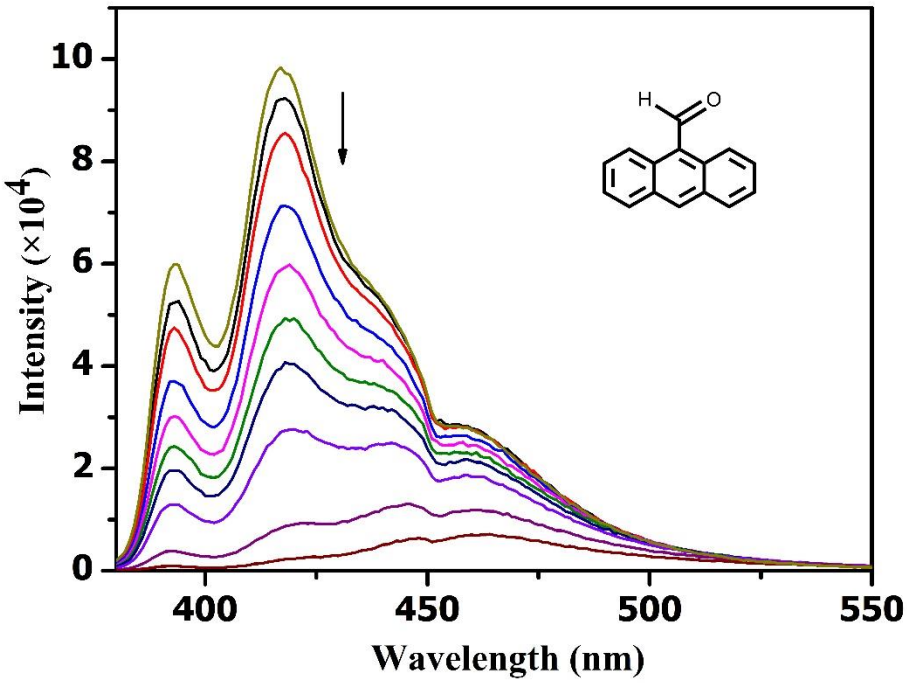

Figure S32. Emission spectra of **1-Co** titrated with 9-anthraldehyde. The arrow indicates a gradual increase of 9-anthraldehyde equivalent.

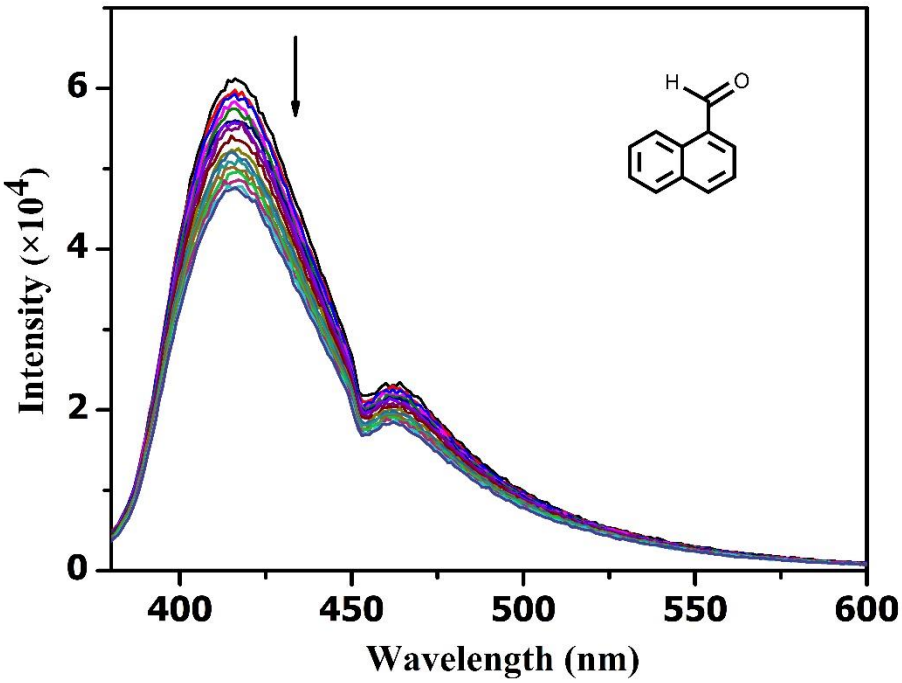

Figure S33. Emission spectra of **1-Zn** titrated with 1-naphthaldehyde. The arrow indicates a gradual increase of naphthaldehyde equivalent.

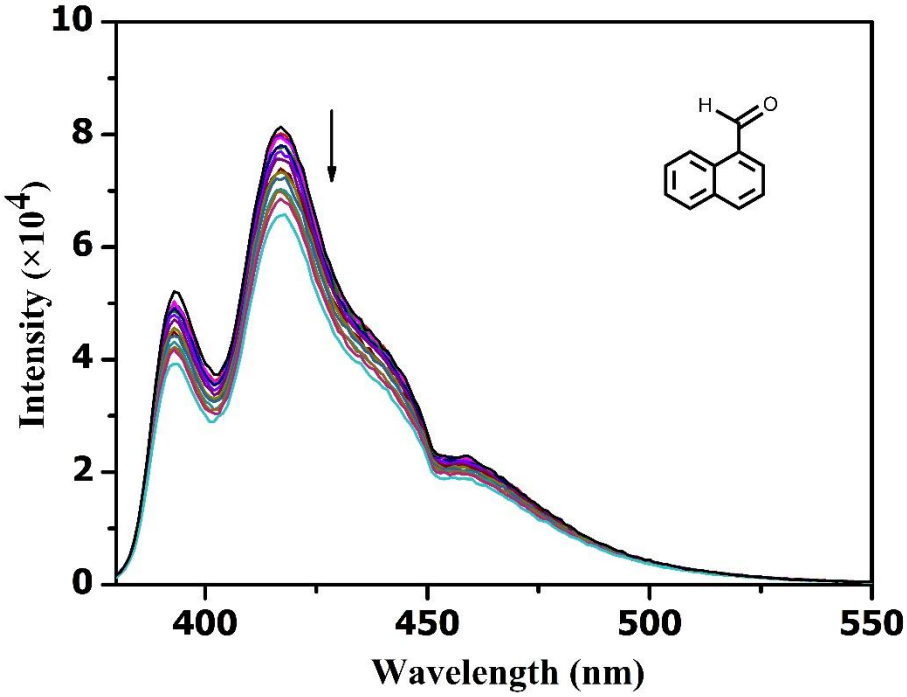

Figure S34. Emission spectra of **1-Co** titrated with 1-naphthaldehyde. The arrow indicates a gradual increase of naphthaldehyde equivalent.

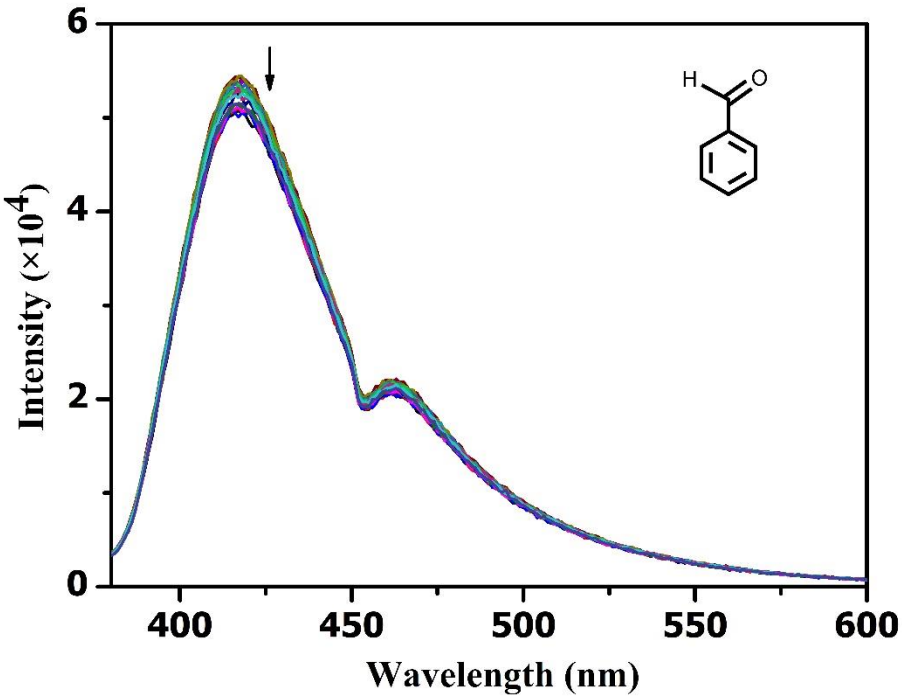

Figure S35. Emission spectra of **1-Zn** titrated with benzaldehyde. The arrow indicates a gradual increase of benzaldehyde equivalent.

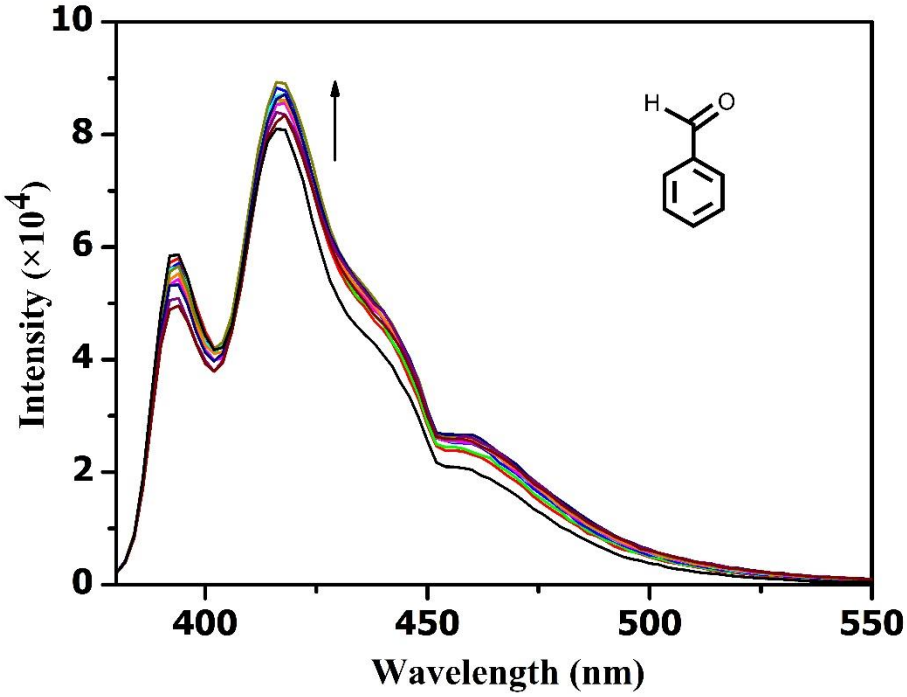

Figure S36. Emission spectra of **1-Co** titrated with benzaldehyde. The arrow indicates a gradual increase of benzaldehyde equivalent.

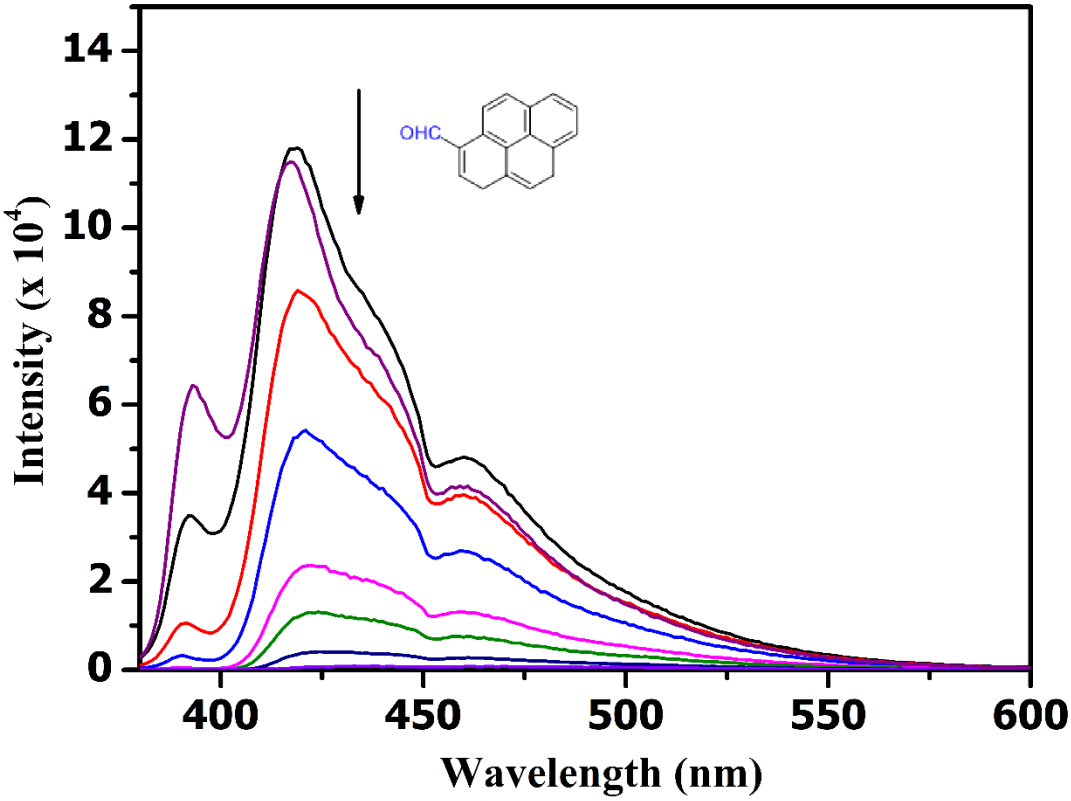

Figure S37. Emission spectra of CF_3COOH-treated **1-Co** titrated with 1-pyrenealdehyde; the arrow indicates a gradual increase of 1-pyrenealdehyde equivalent. The result indicates that 1-pyrenealdehyde is competing with CF_3COOH for the H^+-binding sites, causing the fluorescent emission to reverse.